ADVANCED MATERIALS
www.advmat.de

www.MaterialsViews.com

Tailoring Interface Structure in Highly Strained YSZ/STO Heterostructures

A. Rivera-Calzada, M. R. Diaz-Guillen, O. J. Dura, G. Sanchez-Santolino, T. J. Pennycook, R. Schmidt, F. Y. Bruno, J. Garcia- Barriocanal, Z. Sefrioui, N. M. Nemes, M. Garcia-Hernandez, M. Varela, C. Leon, S. T. Pantelides, S. J. Pennycook,* and J. Santamaria**

Heterostructures combining transition metal oxides, as compared to other materials, are able to accommodate very large amounts of epitaxial strain without breaking into islands or structural domains. Coherently strained interfaces are an interesting playground for the search of materials with enhanced ion diffusivities, of interest in devices for energy generation and storage. In this work we highlight the importance of the interface structure of highly strained YSZ/STO superlattices in determining an enhancement of their ionic conductivity. We show the role of growth orientation in controlling the structure and morphology of the interface. Results of density functional theory calculations are discussed, showing that the incompatibility of the oxygen positions at the interface planes plays a key role in stabilizing the high values of ionic conductivities.

1. Introduction: Strain at Correlated Oxide Interfaces

Correlated transition metal oxides are a wide family of materials which display a number of different electronic ground states: ferromagnets, multiferroics, superconductors and mixed or ionic conductors. Many share a perovskite structure in which the basic building blocks are the oxygen octahedra in which the transition metal is surrounded by oxygen ions. Recent research has shown that heterostructures combining these materials can yield a variety of interesting behaviours resulting from the competition and interplay among different phases at the interfaces.[1] A paradigmatic case is the metallic state at the LAO/STO interface, whose origin is still under debate.[2] This finding, however, has triggered the launch of a truly new research field aimed at finding interesting novel phases at the interfaces with high potential for applications in oxide electronics.[3–5] At interfaces, the important quantities controlling the nucleation of different phases (charge density, electrostatic repulsion and band width) may change substantially in a phenomenon called electronic reconstruction.[6,7] Interface strain is also an important parameter controlling phase stabilization[8] allowing changes in the orbital and spin structures.[9–12]

In connection with epitaxial strain it is quite remarkable that oxides, as compared to other materials, are able to accommodate very large amounts of epitaxial strain without breaking into islands or structural domains. It is quite common that layers with a thickness of several tens of nanometers are referred to as being "uniformly strained" by a substrate with a relatively large mismatch. The reason is probably related to the large polarizability of the oxygen sublattice[7] which admits quite large deformations in the form of rotations and distortions of the oxygen octahedra, allowing the lattice parameter to change with little changes of the bond lengths within individual octahedra. These rotations and distortions do however cause quite substantial changes in the oxygen bond angles, which control the electron hopping rate and consequently the band width W, one of the important energy scales governing phase stabilization. In this regard, it has been proposed that the coherent growth of strained interfaces in heterostructures combining materials with different degrees of lattice mismatch may promote ion diffusivity[13] and thus, these heterostructures may play an important role in the optimization of materials for energy generation and storage. This is the case of the Y_2O_3-ZrO_2/$SrTiO_3$

Dr. A. Rivera-Calzada, Dr. M. R. Diaz-Guillen, Dr. O. J. Dura, Dr. R. Schmidt, Dr. F. Y. Bruno, Dr. J. García- Barriocanal, Dr. Z. Sefrioui, Dr. N. M. Nemes, Dr. C. Leon, Prof. J. Santamaria
GFMC, Departamento de Física Aplicada III, Facultad de Física
Universidad Complutense de Madrid
Campus Moncloa, 28040 Madrid, Spain
E-mail: jacsan@fis.ucm.es

Dr. M. Garcia-Hernandez
Instituto de Ciencia de Materiales de Madrid
Consejo Superior de Investigaciones Cientificas
28049 Cantoblanco, Spain

T. J. Pennycook, Prof. S. T. Pantelides
Department of Physics and Astronomy
Vanderbilt University
Nashville Tennessee 37235, USA
E-mail: pantelides@Vanderbilt.Edu

G. Sanchez-Santolino, Dr. M. Varela, Dr. S. J. Pennycook
Materials Science and Technology Division
Oak Ridge National Laboratory
Oak Ridge, Tennessee 37831-6071, USA
E-mail: pennycooksj@ornl.gov

DOI: 10.1002/adma.201102106

(YSZ/STO) superlattices where different structures (fluorite vs. perovskite) are combined with a large lattice mismatch of 7%. The interface between highly dissimilar structures stabilizes a disordered oxygen sublattice with an increased number of oxygen vacancies which promote oxygen diffusion. This will be the main focus of this article where we will describe recent progress showing the effect of the growth direction in stabilizing different morphologies and degrees of oxygen mobility enhancement.

YSZ is a well known oxygen ion conductor, where oxygen vacancies are introduced by aliovalent substitution of Zr by Y. The substitution of Zr in a 4+ oxidation state by Y^{3+} produces an oxygen vacancy for every two Y atoms. Y substitution stabilizes a cubic fluorite structure in which oxygen occupies the tetrahedral sites of the cubic unit cell. It is technologically a very relevant material for its use in solid oxide fuel cells (SOFC) as an electrolyte.[14] The high operation temperature necessary to minimize ohmic losses limits the range of applications and has stimulated a significant effort to reduce it. Approaches making use of confinement effects in nanostructures (nanoionics) to improve the device performance have emerged as an interesting alternative.[15] Decreasing the size of the system to the nanometer lengthscale leads to a dominant influence of the interfaces on the overall ionic conductivity of the system. Novel phases can be stabilized with enhanced carrier densities and eventually also with enhanced mobilities. It is now widely accepted that nano-size effects in conventional ionic conductors can provide novel routes to achieve higher ionic conductivities.[15] An interesting class of nanoionic phenomena are the space charge effects which occur when sample dimensions become comparable to the space charge length, which is the length scale for charge inhomogeneities. It is well known that the energy for defect generation may be different at surfaces or boundaries. There, an accumulation of defects may occur which in ionic compounds breaks the charge neutrality, which is allowable below the Debye length. The accumulation of defects will create an electric field which will limit further accumulation or will be screened by (other) mobile charges. The discontinuity of the free energy at interfaces naturally results in charge transfer processes which break charge neutrality and may profoundly change the carrier density if the characteristic sample dimension is comparable to the Debye length. A paradigmatic example is the case of CaF_2 and BaF_2 heterostructures,[16] where fluorine ions are transferred from the BaF_2 into the CaF_2 and vacancies in the BaF_2 give rise to enhanced ionic conductivity over a length scale corresponding to the Debye length.

The existence of these size effects in YSZ has been a subject of considerable debate recently due to the small values (0.1 nm) expected for the Debye length based on the large density of carriers. Results on polycrystalline samples deposited by spin coating on sapphire show an enhancement of the ionic conductivity when thickness is reduced.[17] In contrast, other authors have reported a decrease of the ionic conductivity of samples deposited by pulsed laser deposition (PLD) on MgO substrates.[18] The situation when the layers are epitaxial seems to be different. Quite significant enhancements have been reported in the case of epitaxial YSZ layers on MgO when the thickness is as small as 15 nm.[19] The enhancement becomes stronger when thickness is reduced pointing to an interface mechanism which might be absent in the case of polycrystalline samples. More recently, in an attempt to isolate this interface mechanism we grew highly strained heterointerfaces combining ultrathin YSZ and STO layers and found large conductivity values from dielectric spectroscopy measurements, which we attributed to enhanced oxygen conductivity.[13] The dc conductivity determined by ac methods scaled with the number of interfaces and was independent of the YSZ layer thickness, which was taken as an indication of its interfacial origin. Guo has proposed[20] the electronic origin of the large conductivity values found in this experiment, however, we eliminated the possibility that the enhanced conductivity originated in electron doping of the substrate or STO layers by measuring the dc (electronic) contribution of the conductivity, which turned out to be almost three orders of magnitude smaller than the global conductivity measured with ac methods. Other authors have reported smaller conductivity enhancements in PLD grown samples with partially or non coherent interfaces.[21] Cavallaro et al.[22] have grown YSZ/STO heterostructures with 1 nm thick STO using PLD. The layers were discontinuous and YSZ islands had mixed crystalline orientations. They found enhanced values of the electronic conductivity which they attributed to an interfacial alloyed oxide resulting from zirconium/strontium intermixing.

2. Growth and Structure. Controlling Strain Relaxation

Interestingly, we found that changing the YSZ growth direction allows control of the continuity, morphology and epitaxy of the layers, resulting in very different electrical properties. Samples were grown on ⟨001⟩ oriented STO substrates using a high-pressure (2.9 mbar) pure oxygen sputtering system at a substrate temperature of 900 °C. After growth samples were cooled to 700 °C. At this temperature the chamber was filled with 900 mbar O_2 and samples were annealed for 15 minutes before completing the cooling process. This technique has proven to be very adequate for the growth of epitaxial layers of transition metal oxides.[11–13] The crystalline structures of both materials, one being fluorite (YSZ) and the other perovskite (STO) with rather different lattice parameters (a = 5.14 Å for YSZ vs a = 3.90 Å for STO), are at a first sight strongly dissimilar. However, rotating the crystals 45° about the ⟨001⟩ axis allows the coherent growth of both materials along the ⟨001⟩ direction with a 7% lattice mismatch growth if the YSZ layers are thin enough. This is a very large strain level for which relaxation through misfit dislocations is expected according to theories of strain relaxation.[23] On the contrary, we find that for ⟨001⟩ oriented growth a two dimensional epitaxial growth mode occurs. Growth conditions could be tuned to choose between ⟨001⟩ and ⟨110⟩ orientations. Essentially we find that slow deposition at high temperatures promotes the ⟨001⟩ growth, while ⟨110⟩ shows up at larger growth speeds and lower temperatures.

We first discuss the ⟨001⟩ growth. The X-ray diffraction pattern from a conventional X-ray source for a single YSZ film grown on STO shows that the growth is predominantly ⟨001⟩ (see **Figure 1**a). Detailed structural characterization using X-ray diffraction, X-ray reflectivity and X-ray reciprocal space maps was performed in a four-circle Philips X´pert-PRO MRD

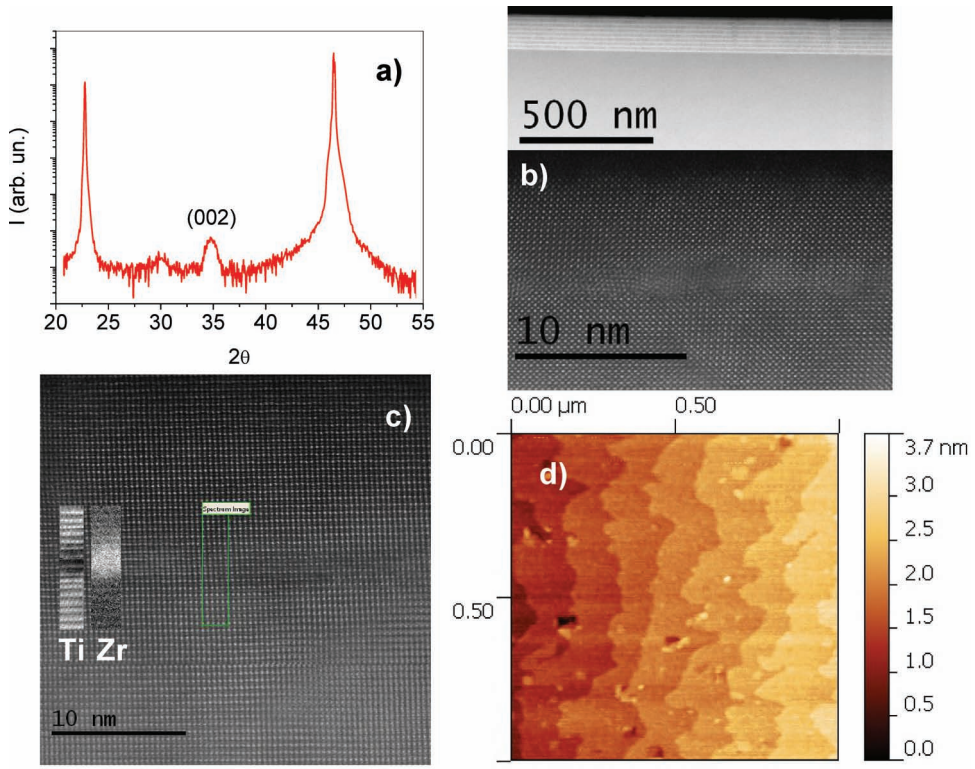

Figure 1. a) XRD pattern of a YSZ thin film of 8 nm showing the epitaxial growth of the YSZ on top of STO with the (001) orientation. b) Low magnification (top) and high resolution of STEM image of a 3 nm YSZ/ 10 nm STO superlattice with 8 bilayer repetitions showing continuous layers and the coexistence of epitaxially coherent and rotated domains. c) High resolution STEM image of a fully strained trilayer of STO/YSZ/STO with a superimposed Ti $L_{2,3}$ and Zr $M_{2,3}$ EELS maps of the area highlighted (spectrum image), acquired with an exposure time of 50 ms per pixel, evidencing the presence of YSZ in the 2 nm ultra-thin layer. All EELS images were produced by integrating the signal under the respective edges after background subtraction using a power law fit and also after applying PCA to the raw data to remove random noise. d) AFM image of a ultra-thin film of 1 nm YSZ grown on top of Nb doped STO.

diffractometer with Cu cathode (wavelength $\lambda = 0.15418$ nm). Note that the (002) reflection of the YSZ at $2\theta = 34.8°$ appears with the highest intensity although the minor presence of a (111) reflection at $2\theta = 30°$ suggests some degree of polycrystalline growth when the thickness increases. Scanning transmission electron microscopy (STEM) and electron energy loss spectroscopy (EELS) measurements were performed on a Nion UltraSTEM operated at 100 kV using a cold field emission electron source, a corrector capable of neutralizing up to fifth order aberrations[24] and an Enfina EEL spectrometer. Some images were also obtained on a VG Microscopes HB501UX with a third order Nion aberration corrector. Samples for STEM were prepared in cross section geometry by conventional thinning, dimpling, and ion milling. The samples were tilted in the microscope to either the ⟨001⟩ or ⟨110⟩ cubic zone axis of STO. The principal component analysis (PCA) method of Ref.[25] was used to eliminate noise in atomic-resolution EELS elemental maps as described in Ref.[26]. Low magnification STEM images of a superlattice with 10 nm thick STO and 3 nm thick YSZ show that interfaces are flat and layers are continuous over long lateral distances (top of Figure 1b). The same figure (bottom panel), displays high magnification STEM images of the same sample showing coherent regions with no structural discontinuity on passing through the interface, coexisting with others where a different orientation of the YSZ starts nucleating. This is consistent with the observation of reflections other than {002} appearing in X-ray diffraction spectra. In Figure 1c, an atomic force microscopy (AFM) image of 1 nm thick layers grown on TiO_2 terminated 0.1% wt. Nb doped STO shows well defined steps one unit cell high separating vicinal terraces indicating a two dimensional growth mode in this thickness range. This tendency is confirmed in the growth of heterostructures with ultrathin YSZ layers sandwiched between STO. Figure 1d shows a high magnification STEM image of a trilayer made with 1 nm thick YSZ in which the YSZ layer is fully epitaxial. Little composition contrast can be observed in the Z contrast images, but EELS elemental maps of the Ti $L_{2,3}$ and Zr $M_{4,5}$ edges confirm the presence of the YSZ layer.

Superlattices made by alternating 1 nm YSZ and 10 nm STO layers were examined by X-ray diffraction at the beamline BM25B of the European Radiation Synchrotron Facility (Grenoble). **Figure 2** displays X-ray diffraction spectra from a synchrotron x ray source (wavelength $\lambda = 0.855$ Å) of a superlattice with 10 nm thick STO and 1 nm thick YSZ layers are displayed in Figure 2. The many (sharp) superlattice satellites are consistent with the good epitaxial properties also shown by the aberration corrected STEM images. The in plane growth was investigated by reciprocal space maps around reflections

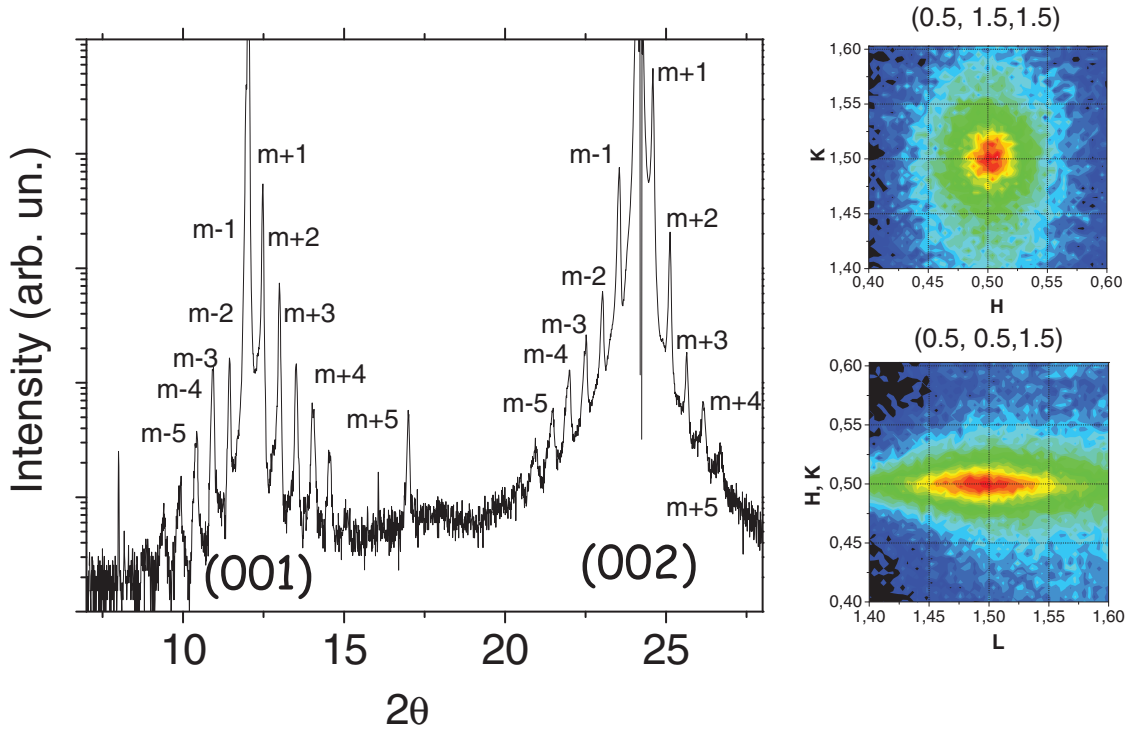

Figure 2. a) Synchrotron X-ray diffraction pattern ($\lambda = 0.855$ Å) obtained at the BM 25 of the the ESRF of a 1 nm YSZ/10 nm STO superlattice with 20 bilayer repetitions s. b) Reciprocal space maps referred to the STO structure in the 0.5 1.5 0.5 (top) and 0.5 0.5 1.5 (bottom) positions, showing the YSZ is forced to the lattice parameters of the STO.

specific for the YSZ and forbidden for the STO, which appear at reciprocal space sites with half integer indexes in STO reciprocal space coordinates. Figures 2b and c show a H vs K and H = K vs L maps of the YSZ layers at half-integer values for the STO, evidencing that the YSZ is fully strained to the lattice parameters of the STO, in a growth mode with the perovskite unit cell rotated 45 degrees to match the half diagonal fluorite cell.

The samples grown with YSZ in a ⟨110⟩ orientation were grown at higher deposition rates. Epitaxy is in principle also possible with {110} planes of the STO matching the {002} planes of the YSZ, and the ⟨110⟩ direction of the YSZ parallel to the ⟨001⟩ direction of the STO. The X-ray diffraction patterns of individual YSZ layers grown on STO (**Figure 3a**) show the highest intensity for the YSZ {110} reflection at $2\theta = 50°$. Also in this case other reflections appear for large film thickness. In this case the AFM observation showed a much stronger tendency to island growth (Figure 3b). None of the AFM observations showed the substrate terrace replication characteristic of 2D growth found in the case of ⟨001⟩ growth. Although overall the lattice mismatch is the same for the ⟨001⟩ growth, there is a strong mismatch between the oxygen sublattices of both materials in this case, which most likely causes the island growth described below. X-ray diffraction patterns of superlattices displayed also superlattice satellite peaks evidencing a certain degree of structural coherence. STEM imaging of these samples showed island growth (Figure 3c and d). Most of the islands appear to be connected but there are changes of the crystalline orientation from island to island. High resolution imaging (Figure 3d) also shows the presence of coherent islands or even larger areas in which the YSZ is strained to match the STO lattice. The chemical integrity of the layer and the connectivity between neighboring islands was checked using EELS elemental maps constructed by integrating intensities of the O K, Zr $M_{2,3}$ and $M_{4,5}$, and Ti $L_{2,3}$ edges. The surface of these islands appears be flat (0.5 nm root mean squared (rms) roughness) over length scales of 1 micrometer, as evidenced by AFM observations. In addition, the growth of the STO on top of the YSZ islands seems to have a flattening effect, such that the growth of the different YSZ layers in superlattices always starts from a flat STO layer. This is most likely the origin of the structural coherence evidenced by x- ray diffraction spectra of these superlattices showing a large number of sharp satellite peaks. Structurally, these samples resemble those grown by Cavallaro et al.[22] by PLD, but differ morphologically in that the YSZ layers are quasi-continuous in our case.

3. Ion Transport at the Interface. Understanding the Mechanism

Conductivity was measured using an alternating current (ac) impedance spectroscopy method (NOVOCONTROL Alpha analyzer) with two evaporated silver spots on the surface as contact electrodes annealed at 220° C. Ac electrical conductivity spectra from impedance spectroscopy experiments displayed strong suppression of the conductivity at low frequencies

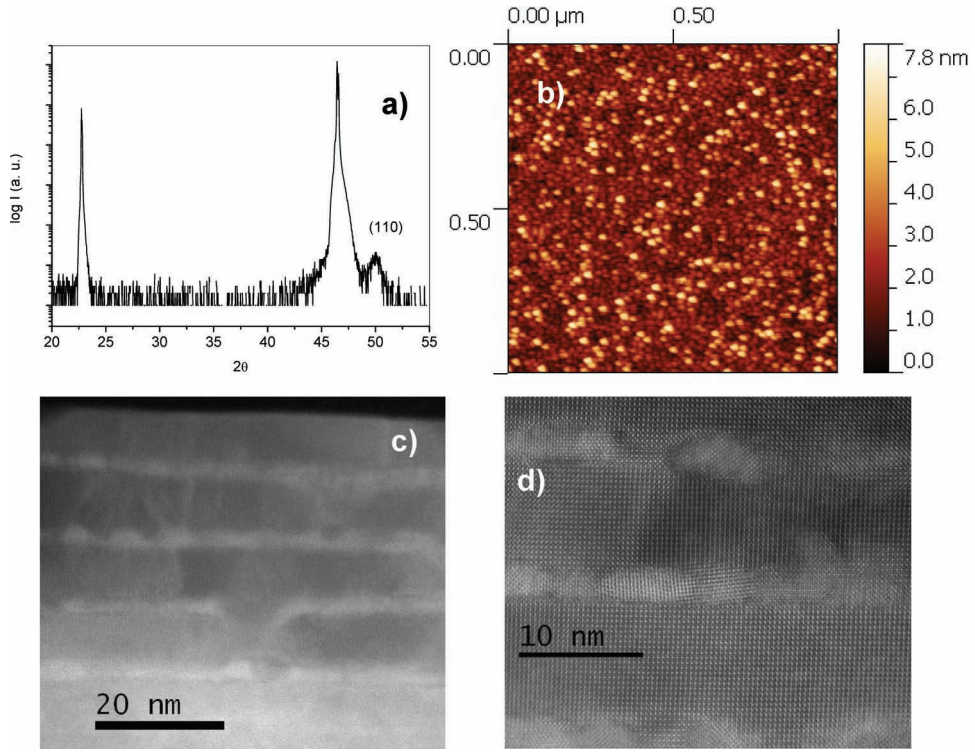

Figure 3. a) XRD pattern of a YSZ thin film of 8 nm showing the epitaxial growth of the YSZ on top of STO. c) AFM image of a thin film of 17 nm YSZ grown on STO showing the grain structure. Low magnification c) and high resolution d) of STEM image of a superlattice of YSZ/STO with 4 bilayers. In d) structural domains with different crystalline orientations are observed, reflecting a non epitaxial growth.

accompanied by up to four orders of magnitude capacitance increases (see right panel of **Figure 4**).

This behaviour is characteristic of blocking of ionic charge carriers at grain boundaries or electrodes. The dc conductivity σ_{dc}, was determined from the frequency independent conductivity plateaus in the spectra.[13] Note that the large conductivity increase (up to 8 orders of magnitude) observed for the fully epitaxial samples results both from an increase of the conductivity pre-exponential factor and from a decrease of the activation energy from values of about 1 eV for bulk samples to 0.6 eV for the ultrathin trilayers.

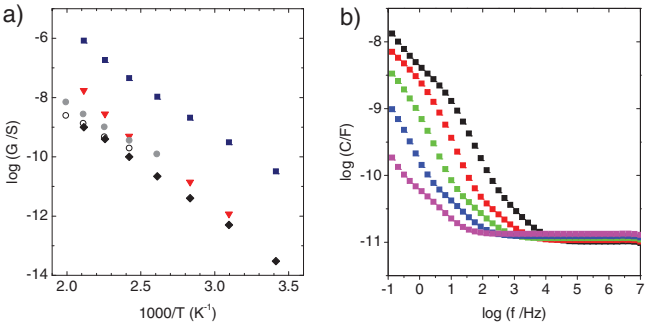

Figure 4. a) Temperature dependence of the conductance for different YSZ/STO heterostructures (trilayers and a superlattice): square symbols correspond to fully epitaxial samples, open and solid circles correspond to relaxed samples with (110) oriented YSZ layers. Diamonds are plain STO substrates and down triangles are STO (bi)layers on STO. b) Frequency dependence of the capacitance of the fully strained superlattice at temperatures 200, 170, 140, 110 and 80 C (from right to left).

The electrical properties of both ⟨001⟩ and ⟨110⟩ oriented YSZ samples are very different. While ⟨001⟩ samples show large values of dc conductivity as compared to conductivity data measured for a bare STO substrate (see Figure 4), ⟨110⟩ samples show conductivity values which resemble more what we find for single substrates. As done previously in reference[22] we have also included in Figure 4 data for STO bilayers grown on STO by interrupting the growth between the STO layers for several minutes. STO bilayers showed similar conductance values to the superlattices with ⟨110⟩ oriented YSZ. Larger conductivities were found in some of the samples with ⟨110⟩ YSZ suggesting that a percolation of the current between islands may be possible in some cases, although the smaller conductivity of those samples indicates that ionic diffusion is blocked by the granular structure.

The enhanced ionic mobility has been discussed in terms of the disorder introduced in the oxygen sublattice by epitaxial strain at the heterointerfaces. Density-functional calculations have been used to investigate the influence of the (001) oriented interface on the conductivity increase in YSZ/STO superlattices.[27] The authors of that work proposed that the combination of epitaxial strain and oxygen sublattice incompatibility between both structures are key in yielding the highly conducting interface. They report that 7% strain produces a drastic change in the O sublattice of YSZ, which becomes as disordered

as expected from an increase of the temperature up to 2000 K. The O ion mean square displacement (mobility) is strongly enhanced (by a factor of over 10^6) as a result of the combined presence of oxygen vacancies and disorder. The incompatibility of the oxygen positions in the interface planes are proposed to play a key role in stabilizing the highly conducting interface. O atoms occupy sites that are close to tetrahedral positions in YSZ. On the other hand, O atoms in STO occupy octahedral positions. The STO structure is more stable than the 7% strained ultrathin YSZ and in turn controls the positions of the O atoms in the YSZ interfacial plane, forcing them all to occupy octahedral positions. This constraint then disturbs the O atoms in the neighboring layers of YSZ with no Ti atoms, causing the extreme disorder in the oxygen sublattice in the region close to the interface. EELS experiments (both spectroscopy and imaging) have provided evidence for the oxygen disorder.[28] The fine structure of the O K edge corresponding to coherent YSZ/STO interfaces has been reported to be blurred out compared to that of bulk YSZ. In addition the O K edge was used to do EELS elemental mapping of individual O columns in bulk cubic YSZ and in YSZ/STO heterostructures. The fact that EELS elemental mapping of coherent regions of YSZ/STO multilayers show clear O columns in the STO, but essentially only a blur in the YSZ, is strong evidence for the presence of O disorder in the strained multilayer YSZ. Moreover, density functional simulations show that a new YSZ phase is stabilized for the epitaxially strained heterostructures for mismatch strain levels in excess of 5.2%.[27] This result explains in fact why these high levels of strain do not result in strain relaxation by mismatch dislocations and islanding and evidences that lattice relaxation plays a dominant role in phase stabilization.

Other ab initio simulations based on combined density functional theory and nudged elastic band method[29] have found an exponential increase of oxygen diffusivity of almost four orders of magnitude in 4% biaxially strained YSZ. This suggests that lattice strain alone cannot be responsible for the large conductivity increases found experimentally. Notice also in this regard that phenomenological models estimating the conductivity increase only on the basis of elastic strain due to lattice mismatch fail in reproducing the large enhancements of the conductivity observed experimentally, suggesting that the relaxation into the oxygen disordered phase is key in understanding the conductivity increase. Korte and co-workers, from a qualitative model of ion diffusion along hetero-interfaces based on the density of misfit dislocations and the interfacial strain have pointed out that strain by itself can only account for 2–3 orders of magnitude conductivity increase.[21] This model predicts for an oxygen vacancy ion conductor a linear increase of the conductivity with lattice mismatch for tensile strained interfaces while compressive strain will decrease the ionic conductivity. However this model does not consider strain relaxation and anisotropy and also does not take into account an interface sheet with enhanced conductivity.

The large conductivity preexponential factor of the trilayer samples, $10^7\ \Omega^{-1}\ cm^{-1}$, which is about 2 orders of magnitude larger than in the single crystal samples ($>10^4\ \Omega^{-1}\ cm^{-1}$), may provide a hint on the importance of disorder to understand the conductivity increase. The conductivity pre-exponential factor is customarily described in terms of the following expression

$$\sigma_\infty = \frac{4\alpha e^2 a^2 v_0 N e^{S/k_B}}{k_B} \quad (1)$$

where α is a geometrical factor, a is the jump distance, v_0 is the attempt frequency, N is the concentration of oxygen vacancies, S is a configurational entropy term, e is the electron charge and k_B is Boltzmann's constant. Either an increase in the concentration of oxygen vacancies (N), or of a larger entropy term ($\exp(S/k_B)$) could in principle be invoked to explain this difference. Most likely a combination of both factors is at play. However, in view of the very high doping level of bulk YSZ it is hard to believe that the carrier density could be further increased by two orders of magnitude. On the other hand, the disorder of the oxygen sublattice obtained from density functional simulations and confirmed experimentally by EELS imaging, provides a firm footing for an increased number of available positions for the oxygen ions (enhanced positional disorder for the oxygen vacancies). Interestingly, the large values of the pre-exponential factor of about $10^7\ \Omega^{-1}\ cm^{-1}$ are not unrealistic. They are in fact comparable to those found in other ion conductors such as β-AgI (showing a value of the pre-exponential factor of $10^8\ \Omega^{-1}\ cm^{-1}$ in which the high mobility phase occurs as a result of the melting of the moving sublattice.[30] The disordered oxygen structure therefore accounts both for the increase of the mobility (reduction of the activation energy) and for the increase of the pre-exponential factor. This constitutes one of the very few cases where the disorder occurring at the interfaces of thin film epitaxial structures yields an improvement of the system properties, instead of a deterioration observed in most practical examples.

As previously mentioned, in addition to the high values of the pre-exponential factor, it is also found in experimental data a decrease of the activation energy from values of about 1 eV for bulk samples to 0.6 eV for the ultrathin trilayers (Figure 4). It is worthwhile to remark in this regard a recent work[30] where a reduction of the activation energy for oxygen ion diffusion has been obtained from an ab initio-based kinetic Monte Carlo model for ionic conductivity in YSZ. According to this model, ionic interactions are found to be essential in reproducing the effective activation energy[31] and the enhanced oxygen ion mobility may result from a non-random distribution of the dopant Y ions at the interfacial planes.[32] There is also evidence from a recent atomistic simulation study of the importance of structural disorder in determining ionic transport properties in YSZ films with nanoscale thickness,[33] where the interfacial conductivity was found to increase by 2 orders of magnitude as the YSZ film size decreases from 9 to 3 nm due to a decrease in the activation energy barrier.

4. Summary and Outlook

In summary, we have discussed how the coherent growth of strained interfaces in heterostructures combining materials with different degrees of lattice mismatch may promote ion diffusivity and thus, these heterostructures may play an important role in the optimization of materials for energy generation and storage. In particular, we have outlined the influence of the growth conditions on the interface structure of highly strained

YSZ/STO superlattices. Controlling the orientation of the YSZ growth has allowed stabilizing different morphologies, layer continuity and epitaxy and, as a result, different degrees of ion mobility enhancement. ⟨001⟩ YSZ growth yields coherent interfaces between both highly dissimilar structures, stabilizing a disordered oxygen sublattice with an increased number of accessible positions for oxygen which promote oxygen diffusion. On the other hand, the ⟨110⟩ YSZ orientation results in the growth of connected islands, whose boundaries block the long range ion diffusion. In addition to space charge effects, epitaxial strain may be thus an important parameter in designing a high mobility landscape at the interfaces.[34]

The wide spread application of the current solid oxide fuel cells devices is limited by the high operation temperatures. An effort is necessary to increase the conductivity of the electrolyte to minimize ohmic losses at lower temperatures. Either new materials have to be sought with optimized conductivity values or new device concepts have to be developed. Definitely, interface effects in epitaxial ionic conducting heterostructures appear as a promising pathway towards novel artificial electrolytes for cooler fuel cells or other electrochemical devices.

However, single chamber fuel cell concepts are necessary to exploit the enhanced interfacial mobility in practical devices. Further work is warranted[35] to asses spectroscopically the nature of the charge carriers responsible for the enhanced conductivity. This is a major experimental challenge in the case of ultrathin layers. Tracer diffusion experiments with isotopically modified ions will be useful to make this point clear. In addition, as pointed out in this work, the predictive power of first principles tools may be determinant in the design of optimized interfaces for application in practical devices.

Acknowledgements

Work at UCM supported by Spanish MICINN Grant MAT 2008 06517, Consolider Ingenio CSD2009-00013 (IMAGINE), CAM S2009-MAT 1756 (PHAMA) and the European Research Council Starting Investigator Award "STEMOX". Work at ORNL was supported by the Materials Sciences and Engineering Division, Office of Basic Energy Sciences, U.S. Department of Energy. Research at Vanderbilt was supported in part by the U. S. Department of Energy Grant DE-FG02-09ER46554 and the McMinn Endowment. R.S. & N.M.N. Spanish thank MICINN for granting Ramon y Cajal Fellowships. O.J.D thanks JCCM for a post doc Fellowship.

Published online: October 4, 2011

[1] E. Dagotto, *Science* **2005**, *309*, 257.
[2] A. Ohtomo, H. Y. Hwang, *Nature* **2004**, *427*, 423.
[3] N. Reyren, S. Thiel, A. D. Caviglia, L. Fitting Kourkoutis, G. Hammerl, C. Richter, C. W. Schneider, T. Kopp, A.-S. Ruetschi, D. Jaccard, M. Gabay, D. A. Muller, J.-M. Triscone, J. Mannhart, *Science* **2007**, *317*, 1196.
[4] A. Brinkman, M. Huijben, M. van Zalk, J. Huijben, U. Zeitler, J. C. Maan, W. G. van derWiel, G. Rijnders, D. H. A. Blank, H. Hilgenkamp, *Nat. Mater.* **2007**, *6*, 493.
[5] E. Bousquet, M. Dawber, N. Stucki, C. Lichtensteiger, P. Hermet, S. Gariglio, J. M. Triscone, P. Ghosez, *Nature* **2008**, *452*, 732.
[6] S. Okamoto, A. Millis, *Nature* **2004**, *428*, 630.
[7] J. Mannhart, D. G. Schlom, *Science* **2010**, *327*, 1607.
[8] a) Y. Tokura, N. Nagaosa, *Science* **2000**, *288*, 462; b) S. Okamoto, A. J. Millis, *Nature* **2004**, *428*, 630.
[9] J. Chakhalian, J. W. Freeland, G. Strajer, J. Strempfer, G. Khaliullin, J. C. Cezar, T. Charlton, R. Dalgliesh, C. Bernhard, G. Cristiani, H. U. Habermeier, B. Keimer. *Nat. Phys.* **2006**, *2*, 244.
[10] P. Yu, J.-S. Lee, S. Okamoto, M. D. Rossell, M. Huijben, C.-H. Yang, Q. He, J. X. Zhang, S. Y. Yang, M. J. Lee, Q. M. Ramasse, R. Erni, Y.-H. Chu, D. A. Arena, C.-C. Kao, L. W. Martin, R. Ramesh, *Phys. Rev. Lett.* **2010**, *105*, 027201.
[11] J. Garcia-Barriocanal, J. C. Cezar, F. Y. Bruno, P. Thakur, N. B. Brookes, C. Utfeld, A. Rivera-Calzada, S. R. Giblin, J. W. Taylor, J. A. Duffy, S. B. Dugdale, T. Nakamura, K. Kodama, C. Leon, S. Okamoto, J. Santamaria, *Nat. Commun.* **2010**, *1*, 82.
[12] J. Garcia-Barriocanal, F. Y. Bruno, A. Rivera-Calzada, Z. Sefrioui, N. M. Nemes, M. Garcia-Hernandez, J. Rubio-Zuazo, G. R. Castro, M. Varela, S. J. Pennycook, C. Leon, J. Santamaria, *Adv. Mater.* **2010**, *22*, 627.
[13] J. Garcia-Barriocanal, A. Rivera-Calzada, M. Varela, Z. Sefrioui, E. Iborra, C. Leon, S. J. Pennycook, J. Santamaria, *Science* **2008**, *321*, 676.
[14] B. C. H. Steele, A. Heinzel, *Nature* **2001**, *414*, 352.
[15] J. Maier, *Nat. Mater.* **2005**, *4*, 805.
[16] N. Sata, K. Eberman, K. Eberl, J. Maier, *Nature* **2000**, *408*, 946.
[17] H. L. Tuller, *Solid State Ionics***2000**, *131*, 143.
[18] X. Guo, E. Vasco, S. Mi, K. Szot, E. Wachsman, R. Waser, *Acta Mater.* **2005**, *53*, 5161.
[19] I. Kosacki, C. M Rouleau, P. F. Becher, J. Bentley, D. H. Lowdness, *Solid State Ionics* **2005**, *176*, 1319.
[20] X. Guo, *Science* **2009**, *324*, 465.
[21] N. Schichtel, C. Korte, D. Hesse, J. Janek, *Phys. Chem. Chem. Phys.* **2009**, *11*, 3043.
[22] A Cavallaro, M. Burriel, J. Roqueta, A. Apostolidis, A. Bernardi, A. Tarancón, R. Srinivasan, S. N. Cook, H. L. Fraser, J. A. Kilner, D. W. McComb, J. Santiso, *Solid State Ionics* **2010**, *181*, 592.
[23] J. W. Matthews, A. E. Blakeslee, *J. Cryst. Growth* **1974**, *27*, 118.
[24] O. L. Krivanek, G. J. Corbin, N. Dellby, B. F. Elston, R. J. Keyse, M. F. Murfitt, C. S. Own, Z. S. Szilagyi, J. W. Woodruff, *Ultramicroscopy* **2008**, *108*, 179.
[25] M. Bosman, M. Watanabe, D. T. L. Alexander, V. J. Keast, *Ultramicroscopy* **2006**, *106*, 1024.
[26] M. Varela, M. P. Oxley, W. Luo, J. Tao, M. Watanabe, A. R. Lupini, S. T. Pantelides, S. J. Pennycook, *Phys. Rev. B* **2009**, *79*, 085117.
[27] T. J. Pennycook, M. J. Beck, K. Varga, M. Varela, S. J. Pennycook, S. T. Pantelides, *Phys. Rev. Lett.* **2010**, *104*, 115901.
[28] T. J. Pennycook, M. P. Oxley, J. Garcia-Barriocanal, F. Y. Bruno, C. Leon, J. Santamaria, S. T. Pantelides, M. Varela, S. J. Pennycook. *Eur. Phys. J.* **2011**, *54*, 33507.
[29] A. Kushima, B. Yildiz, *J. Mater. Chem.* **2010**, *20*, 4809.
[30] J. Garcia-Barriocanal, A. Rivera-Calzada, M. Varela, Z. Sefrioui, M. R. Diaz-Guillen, K. J. Moreno, J. A. Diaz-Guillen, E. Iborra, A. F. Fuentes, S. J. Pennycook, C. Leon, J. Santamaria, *ChemPhysChem* **2009**, *10*, 1003.
[31] K. L. Ngai, *J. Non-Cryst. Solids* **1996**, *203*, 232.
[32] E. Lee, F. B. Prinz, W. Cai, *Phys Rev. B* **2011**, *83*, 052301.
[33] S. K. R. S. Sankaranarayanan, S. Ramanathan, *J. Chem. Phys.* **2011**, *134*, 064703.
[34] E. Fabbri, D. Pergolesi, E. Traversa, *Sci. Technol. Adv. Mater.* **2010**, *11*, 054503.
[35] J. A. Kilner, *Nat. Mater.* **2008**, *7*, 838.